JOURNAL OF SPACECRAFT AND ROCKETS
Vol. 31, No. 3, May–June 1994

Aerothermodynamic Methods for a Mars Environmental Survey Mars Entry

R. A. Mitcheltree*
NASA Langley Research Center, Hampton, Virginia 23681

Computational fluid dynamics models for the thermodynamics and transport properties used in an equilibrium version of the Langley aerothermodynamics upwind relaxation algorithm (LAURA) for Mars atmospheric entries are described. In addition, the physical models used in a nonequilibrium version of LAURA for Mars-entry flows are described. Uncertainties exist in defining constants used in the transport properties for the equilibrium model and in many of the physical models for the nonequilibrium version. Solutions from the two codes using the best available constants are examined at the Mars-entry conditions characteristic of the Mars environmental survey mission. While the flowfields are near thermal equilibrium, chemical nonequilibrium effects are present in the entry cases examined. Convective heating at the stagnation point for these flows (assuming fully catalytic wall boundary conditions) is approximately 100 W/cm². Radiative heating is negligible.

Nomenclature

A_s, B_s, C_s	=	curve fit coefficients for viscosity of species s (Eq. 8)
a	=	speed of sound, m/s
a_s, b_s, c_s, d_s, e_s	=	curve fit coefficients for thermal conductivity of species s (Eq. 11)
C_p	=	specific heat at constant pressure, J/kg—K
$C_{p,T}$	=	total specific heat, J/kg—K
c_s	=	mass fraction of species s
D	=	mixture coefficient of diffusion, m_2/s
δ_{shock}	=	shock standoff distance, m
μ	=	viscosity, kg/m—s
$\pi\bar{\Omega}^{1,1}_{s,r}$	=	collision integral for species s, r, m²
$\pi\bar{\Omega}^{2,2}_{s,r}$	=	collision integral for species s, r, m²
ρ	=	density, kg/m³
σ, ϵ/k	=	force constants in Lennard-Jones potential

Introduction

THE NASA Mars environmental survey[1] (MESUR) mission proposes the landing of 16 independent probes on Mars to observe the atmosphere and planetary surface. Accurate description of the aerothermal environment about these probes during entry into the Mars atmosphere is required to design the thermal protection system for their entry aeroshells.

Several recent studies have performed detailed predictions of the aerothermodynamics of entry into the Mars atmosphere.[2-9] References 2 and 3 address the MESUR mission directly.

Two computational procedures which employ a Navier-Stokes solver are developed in the present work which describe the flow about a vehicle entering the Mars atmosphere. The two procedures differ in their modeling of the thermochemical state of the CO_2—N_2 gas. The first assumes equilibrium thermochemistry and defines the thermodynamic state via minimization of Gibb's free energy. The second tool allows both thermal and chemical nonequilibrium in a two-temperature formulation. Both codes are modifications of the Langley Aerothermodynamic Upwind Relaxation Algorithm (LAURA) of Gnoffo et al.[10] and Gnoffo[11] and are capable of handling complex three-dimensional shapes including base flows. The results presented, however, are limited to the axisymmetric blunt forebody flows characteristic of the MESUR mission.

Different trajectories have been proposed for the MESUR entry into the Mars atmosphere.[2,3] Primarily, trajectories differ as a result of uncertainties in the vehicle's geometry and ballistic coefficient as well as variations in the atmospheric interface conditions (i.e., inertial entry velocity and flight-path angle). The present work examines the maximum heating point of two possible trajectories. The first is a 7-km/s ballistic entry with entry flight-path angle of −20 deg and ballistic coefficient of 38.7 kg/m². This trajectory is defined by the three-degree-of-freedom version of the program to optimize simulated trajectories (POST).[12] The maximum stagnation-point heating is predicted to occur at 37.9 km altitude with a relative velocity of 5819 m/s. This estimate is based on an extension of Chapman's cold-wall, convective-heating correlation[13] for the Mars atmosphere. The 70-deg sphere-cone vehicle has a base radius of 1.25 m, nose radius of 0.625 m and a shoulder radius at the base corner of 0.0254 m. Since the geometry for the second trajectory has a different nose radius, the two trajectories are differentiated by reference to their respective geometry's nose radius.

The second trajectory is based on a 7-km/s entry of a 0.85-m base radius MESUR vehicle with ballistic coefficient of 30 kg/m² entering at flight-path angle of −20 deg.[2,3] The maximum heating point for this trajectory is at 41.7 km altitude and a velocity of 6155 m/s. The vehicle has a nose radius of 0.425 m and a shoulder radius of 0.0425 m. This second trajectory will be referred to as the 0.425-m body's trajectory.

Several solutions will be examined at different points on the 0.625-m body's trajectory including the maximum heating point. Only the maximum heating point is examined for the 0.425-m body's trajectory.

Because the Mars atmosphere can be laden with dust following surface wind storms, design of the thermal protection for the MESUR probe should consider the possibility of heat shield erosion due to dust particle impact. Reference 2 concludes, however, that prediction of this effect need not be coupled to the flowfield computation. The present flowfield calculations do not include dust effects.

Received June 3, 1993; presented as Paper 93-2761 at the AIAA 28th Thermophysics Conference, Orlando, FL, July 6–9, 1993; revision received July 19, 1993; accepted for publication Aug. 4, 1993.

*Aerospace Engineer, Aerothermodynamics Branch, Space Systems Division, M.S. 366. Member AIAA.

The objective of the present work is to first describe the physical models (thermodynamics and transport properties) used in each of the two codes (the equilibrium and thermochemical nonequilibrium) for Mars atmosphere flows, then examine solutions from each at points on the MESUR trajectories. When possible, comparisons with other computational results and approximate methods are included. The movement of the sonic line and effect on surface conditions resulting from varying the vehicle's cone half-angle plus or minus one degree are explored.

Equilibrium Thermodynamics

When the elemental concentrations comprising a gas are fixed, the equilibrium thermodynamic state of that gas is a function of two state variables. For the Mars atmosphere, the elemental concentrations of C, O, and N are assumed to be 0.2647, 0.7053, and 0.0300, respectively which is equivalent to freestream mass fractions of 97 percent CO_2 and 3 percent N_2.

The equilibrium code is not restricted to Mars atmospheric constituents. Nineteen species are considered: O, O_2, O^+, O_2^+, N, N_2, N^+, N_2^+, NO, NO^+, C, C_2, C_3, CO, CO_2, CN, C^+, CO^+, and e. From Gupta et al.'s[8,14] curve fits for the specific heats at standard pressure, values for enthalpy, entropy, and molal standard free energy F_s^0 for each species s can be obtained as a function of temperature. The species concentrations and the thermodynamic variables are then computed by Gibb's free-energy minimization. Free energy for the mixture is determined by the pressure and the species mole numbers x_s from

$$F_{\text{mix}} = \sum_{s=1}^{n} x_s \left[F_s^0 + lnP + ln \frac{x_s}{\Sigma x_s} \right] \tag{1}$$

Finding the thermodynamic state for a given pressure and temperature is then a matter of finding that set of mole numbers x_s which minimizes F_{mix}. Stroud and Brinkley[15] used the method of steepest descent applied to a quadratic representation of the free-energy surface to find the minimum energy point on the hyperspace restained by the elemental mass fractions. This approach is employed in the present work.

Equation of State

No explicit equation of state is necessary when free-energy minimization is used to define the thermodynamic state. Significant savings in computational time can occur, however, if the thermodynamics are not calculated every iteration of the governing equations. An equivalent gamma formulation can be used to update the pressure and temperature during those iterations in which the thermodynamics are not recomputed. This approach was used in LAURA for equilibrium air by Greene.[16] The relations are

$$P = (\gamma - 1)\rho e \tag{2}$$

and

$$T = (PM_{\text{mix}})/(\bar{R}\rho) \tag{3}$$

γ is not the ratio of specific heats. In fact, Eq. (2) is the definition of γ. By performing the free-energy minimization calculation (or, for Ref. 16, curve fit evaluations of the equilibrium state) values for γ and M_{mix} are defined at each point in the flowfield. These values are then held constant for the next 20 to 100 updates of the governing equations while pressure and temperature change with changing density and internal energy according to Eqs. (2) and (3).

A variation of Eq. (2) is required for generalized application of this approach to any gas mixture. The variation is required since internal energy e is not strictly positive for all possible elemental compositions. For example, the Mars atmosphere at 97 percent CO_2 has a negative freestream energy since the heat of formation of CO_2 is -93.964 kcal/g—mole. Negative energies alone would not prevent the use of Eq. (2) since negative γ's are possible and would result in finite, positive pressures. The problem for escape velocity entries into Mars like MESUR, is that energies within the shock layer can become positive. Thus at the point where e crosses zero, a continuous P requires γ in Eq. (2) to be unbounded, which precludes numerical treatment.

An alternative to Eq. (2) that circumvents this problem is a different equivalent gamma definition

$$P = (\gamma^* - 1)\rho(e - e_{\infty,0}) \tag{4}$$

where $e_{\infty,0}$ is a constant for the entire flowfield set to the zero point energy of the freestream (or largest negative zero point energy in the flowfield). Here, γ^* can be called the sensible equivalent gamma. The quantity $(e - e_{\infty,0})$ is then strictly positive everywhere in the flowfield so that γ^* can remain finite. The corresponding temperature relation is unchanged. Once a suitable value of $e_{\infty,0}$ is set for the conditions being examined, the free-energy minimization is used to compute γ^* and M_{mix} at every other point in the flowfield and then these values are held constant for 20–100 flowfield equation updates. Originally, the value of the zero-point energy at each point in the flowfield, e_0, was used in place of the constant $e_{\infty,0}$ in Eq. (4). Using the local value was another way of ensuring positive pressures for Mars entry flows. (The quantity $e - e_0$ is the mixture's local sensible energy.) The resulting scheme, however, suffered stability problems. These problems were most likely a result of poor approximations of the pressure derivatives required by the upwind algorithm. The requirements of the algorithm and the pressure derivatives approximated from Eq. (5) which result in a robust scheme are discussed below.

Newton Iteration

Unfortunately the Stroud and Brinkley formulation for free-energy minimization requires specification of P and T [Eq. (1)], which then establishes ρ, e, x_s, etc. Solution of the governing equations, however, provides ρ and e and requires the thermodynamics to then specify P and T, which is opposite of the desired exchange. A Newton iteration is required. In short, suitable guesses at P and T are made until values that produce the latest ρ and e are found.

A Newton iteration to find P and T requires analytic expressions for their derivatives. Since the free-energy minimization process is a numerical procedure, no such analytic expressions exist. Numerical derivatives are computed. This inefficient process makes this calculation computationally expensive.

Upwind Algorithm's Needs

An upwind scheme, like LAURA, which diagonalizes the Jacobian matrix, requires information about the thermodynamics of the mixture. In particular, derivatives of pressure with respect to the conserved variables are required. These derivatives and the speed of sound appear in the definition of the difference equation's eigensystem.

Different methods for obtaining this information were examined including the use of numerically derived derivatives produced as a byproduct of the Newton iteration described. The simplest method, however, is to approximate them from the equivalent equation of state of Eq. (4). In particular, if γ^* is assumed not to be a function of the conserved variables then

$$\frac{\partial P}{\partial \rho} \approx (\gamma^* - 1)(e - e_{\infty,0}) \tag{5}$$

$$\frac{\partial P}{\partial e} \approx (\gamma^* - 1)\rho \tag{6}$$

For the same assumptions, the speed of sound is

$$a^2 = \frac{\gamma^* P}{\rho} \tag{7}$$

These approximations are crude, but numerical experimentations reveal they supply the algorithm with sufficient information about the mixture's thermodynamics.

Equilibrium Transport Properties

In addition to the thermodynamics, the equilibrium method needs transport properties for the mixture. Coefficients of viscosity, thermal conductivity and mass diffusion are required.

Viscosity

Viscosity for species s has been curve fit by Gupta et al.[8,14] The three parameter fits are a function of temperature.

$$\ln \mu_s = A_{s\chi}^2 + B_{s\chi} + C_s \tag{8}$$

where $\chi = \ln T$. The viscosity of the mixture is then computed via Wilke's rule[17]

$$\mu = \sum_s \frac{X_s \mu_s}{\Sigma_j X_j \phi_{s,j}} \tag{9}$$

with

$$\phi_{s,j} = \frac{1}{\sqrt{8}}\left(1 + \frac{M_s}{M_j}\right)^{-1/2}\left[1 + \left(\frac{\mu_s}{\mu_j}\right)^{1/2}\left(\frac{M_j}{M_s}\right)^{1/4}\right]^2 \tag{10}$$

An electron pressure correction is applied for ionized flows.[14]

Thermal Conductivity

Similarly, Gupta et al.[8,14] have curve fit thermal conductivity for each species s as

$$\ln k_s = a_s\psi^4 + b_s\psi^3 + c_s\psi^2 + d_s\psi + e_s \tag{11}$$

The conductivity of the mixture is found by Mason and Saxena's formula[18]

$$k_{\text{mix}} = \sum_s \frac{k_s}{1 + \Sigma_{k,k\neq s} G_{s,k}(x_k/c_k)} \tag{12}$$

where

$$G_{s,k} = \frac{1.065}{2\sqrt{2}}\left(1 + \frac{M_s}{M_k}\right)^{-1/2}\left[1 + \left(\frac{\mu_s M_k}{\mu_k M_s}\right)^{1/2}\left(\frac{M_s}{M_k}\right)^{1/4}\right]^2 \tag{13}$$

The curve fits for individual species viscosity and thermal conductivity are not valid much below 1000 K. Sutherland's law for individual species is used to specify viscosity and thermal conductivity when the temperature is at or below 500 K. In addition, the minimum temperature used in the viscosity and thermal conductivity curve fits for the ionic species is set to 1000 K.

Diffusion

In the conservation of total energy equation, the heat flux is

$$q_j = k_{\text{mix}}\frac{\partial T}{\partial x^j} + \rho\sum_s h_s D_s \frac{\partial c_s}{\partial x_j} \tag{14}$$

where D_s is the coefficient of binary diffusion for species s. This can be rewritten as

$$q_j = \left(k_{\text{mix}} + \rho\sum_s h_s D_s \frac{\partial c_s}{\partial T}\right)\frac{\partial T}{\partial x^j} \tag{15}$$

When combined with

$$\frac{\partial h}{\partial x^j} = \left(C_p + \sum_s h_s \frac{\partial c_s}{\partial T}\right)\frac{\partial T}{\partial x^j} \tag{16}$$

this yields

$$q_j = \frac{\mu}{Pr_T}\frac{\partial h}{\partial x^j} \tag{17}$$

where

$$Pr_T = \frac{\mu C_{p,T}}{k_T} \tag{18}$$

$$C_{p,T} = C_p + \sum_s h_s \frac{\partial c_s}{\partial T} \tag{19}$$

If a total coefficient of diffusion D is defined in

$$\rho\sum_s h_s D_s \frac{\partial c_s}{\partial T} = \rho D \sum_s h_s \frac{\partial c_s}{\partial T} \tag{20}$$

then in terms of the Lewis number L_e,

$$k_T = k_{\text{mix}} + \frac{L_e k_{\text{mix}}}{C_p}\sum_s h_s \frac{\partial c_s}{\partial T} \tag{21}$$

where

$$L_e = \frac{\rho D C_p}{k_{\text{mix}}} \tag{22}$$

If the Lewis number is assumed constant, then Eq. (22) is the definition of D. Results from calculations assuming a Lewis number of 1.4 and 1.0 will be presented. The required derivatives for establishing the reactive contributions to the thermal conductivity and specific heat in Eqs. (19) and (21) are evaluated numerically during the Newton iteration on free-energy minimization.

Nonequilibrium Models

The physical models required by the Mars nonequilibrium calculation include the chemical kinetics, the thermodynamics, the transport properties, and the relaxation processes of the CO_2—N_2 gas mixture. In the present work all of these processes are modeled for the Mars atmosphere in a manner identical to their treatment for air as detailed in Ref. 10. This section will therefore only describe those differences associated with the Mars atmosphere and Ref. 10 should be consulted for the complete details.

Instead of the 11 species, 26 reaction chemical kinetics for air, an eight species (CO_2, CO, N_2, O_2, NO, C, N, and O), 14 reaction set described in Ref. 5 is used.

Thermodynamic relations for this two-temperature nonequilibrium method make use of the same species curve fits for the specific heat as the equilibrium code. Note that the calculation of the thermodynamics is different than that used by Candler.[6] In particular, the vibrational-electronic enthalpy for a molecular species is evaluated by utilizing the curve fit for a specific enthalpy evaluated at the vibrational-electronic temperature T_V and subtracting out both the contribution from the rotational

and translational enthalpy calculated at T_V. Then the specific enthalpy is computed by adding the contribution of translational and rotational enthalpy evaluated at temperature T plus the enthalpy of formation to the vibrational-electronic enthalpy. This approach assumes both the rotational and translational modes are fully excited: a valid assumption for entry flowfields.

As outlined in Ref. 10, all transport properties are evaluated from collision integrals for each species pair. The collision integrals are evaluated from curve fits which assume a linear variation of $\log_{10}(\pi\bar{\Omega}^{1,1}_{s,r})$ and $\log_{10}(\pi\bar{\Omega}^{2,2}_{s,r})$ with ln (T). This linear variation is established by specifying values for the collision integrals at 2000 and 4000 K. The values for the collision pairs involving only the species N_2, O_2, NO, N, and O are taken from Ref. 10. The collision integrals for the remainder of the collision pairs were computed via a Lennard-Jones potential.[19] Values for the force coefficients used in the Lennard-Jones potentials are listed in Table 1. The resulting collision integrals for the remaining pairs are listed in Table 2.

From the collision integrals, binary diffusion coefficients for each species pair are defined. The effective diffusion coefficient of species s in the mixture is then defined as a molal-weighted average of those binary diffusion coefficients which include that species.

Relaxation of vibrational energy into translational modes for each species except CO_2 is modeled by the semiempirical correlation of Millikan and White[20] as is done for air in Ref. 10. For CO_2, an empirical relation established from the data of Camac[21] is used (as is done in Ref. 6).

Preferential dissociation is modeled in the present work in two separate instances. First, $\sqrt{TT_V}$ is used as the rate controlling temperature for the dissociation reactions. Second, molecules are assumed to dissociate or recombine with vibrational energy ten times that of the average vibrational energy for the location of the reaction. The amount of vibrational energy removed or gained from a molecule dissociating or recombining is a matter of debate in the modeling of thermal-nonequilibrium flows.[22] Further discussion of this model is included in the Results section.

Table 1 Force constants used in the Lennard-Jones potential

Species	σ	ϵ/κ
CO_2	3.897	213.0
CO	3.706	88.0
N_2	3.749	79.8
O_2	3.541	88.0
NO	3.599	91.0
C	3.385	30.6
N	3.298	71.4
O	3.050	106.7

Table 2a Collision integrals for Martian atmosphere pairs

Pair		$\log_{10}(\pi\bar{\Omega}^{(2,2)}_{s,r})$ at	
s	r	T= 2000 K	T= 4000 K
N	CO_2	−14.5497	−14.6009
N	CO	−14.6062	−14.6547
N	C	−14.6839	−14.7308
O	CO_2	−14.5659	−14.6169
O	CO	−14.6251	−14.6722
O	C	−14.7028	−14.7503
N_2	CO_2	−14.4926	−14.5447
N2	CO	−14.5483	−14.5964
N2	C	−14.6237	−14.6705
O_2	CO_2	−14.5130	−14.5651
O_2	CO	−14.5698	−14.6175
O_2	C	−14.6458	−14.6928
NO	CO_2	−14.5051	−14.5570
NO	CO	−14.5618	−14.6095
NO	C	−14.6373	−14.6844
CO_2	CO_2	−14.4456	−14.4930
CO_2	CO	−14.4940	−14.5461
CO_2	C	−14.5712	−14.6196
CO	CO	−14.5502	−14.5980
CO	C	−14.6254	−14.6723
C	C	−14.7014	−14.7464

Table 2b Collision integrals for Martian atmosphere pairs

Pair		$\log_{10}(\pi\bar{\Omega}^{(1,1)}_{s,r})$ at	
s	r	T= 2000 K	T= 4000 K
N	CO_2	−14.5022	−14.5498
N	CO	−14.5564	−14.6016
N	C	−14.6316	−14.6755
O	CO_2	−14.5195	−14.5668
O	CO	−14.5760	−14.6201
O	C	−14.6514	−14.6958
N_2	CO_2	−14.4454	−14.4938
N2	CO	−14.4987	−14.5436
N2	C	−14.5717	−14.6153
O_2	CO_2	−14.4661	−14.5145
O_2	CO	−14.5203	−14.5650
O_2	C	−14.5940	−14.6379
NO	CO_2	−14.4583	−14.5065
NO	CO	−14.5125	−14.5570
NO	C	−14.5856	−14.6296
CO_2	CO_2	−14.4006	−14.4445
CO_2	CO	−14.4470	−14.4955
CO_2	C	−14.5214	−14.5666
CO	CO	−14.5008	−14.5454
CO	C	−14.5736	−14.6174
C	C	−14.6472	−14.6871

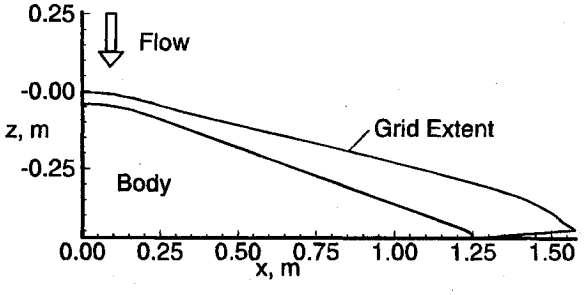

Fig. 1 Axisymmetric geometry of 0.625-m nose MESUR vehicle and extent of 30 × 64 computational grid.

Results

Results from the equilibrium and nonequilibrium calculations are compared at the maximum heating point of the 0.625-m body MESUR Mars-entry trajectory (V_∞ = 5819 m/s, ρ_∞ = 0.44302e—03 kg/m^3, T_∞ = 165 K). The axisymmetric geometry and the extent of the 30 × 64 computational grid (30 cells along the body) are shown in Fig. 1. The cell Reynolds number for the first cell off the wall is set to 1.0. Although no grid studies are included in this paper, the grid is judged as adequate based on past experiences with similar geometries and heating levels.[10]

Comparisons of the surface pressure and convective heating are shown in Figs. 2 and 3. Two equilibrium solutions, Lewis number of 1.4 and 1.0, are included. The pressures predicted by all three calculations agree. The convective heating predictions of the equilibrium code using a Lewis number of 1.0 are within 7 percent of those predicted by the nonequilibrium code. Increasing the Lewis number to 1.4 produces an 18-percent-higher heating prediction. The wall temperature for all three calculations is set to 2000 K which is approximately the radiative equilibrium wall temperature for the heating levels predicted. The nonequilibrium solution assumes the wall to be fully catalytic. In reality, the surface will possess some degree

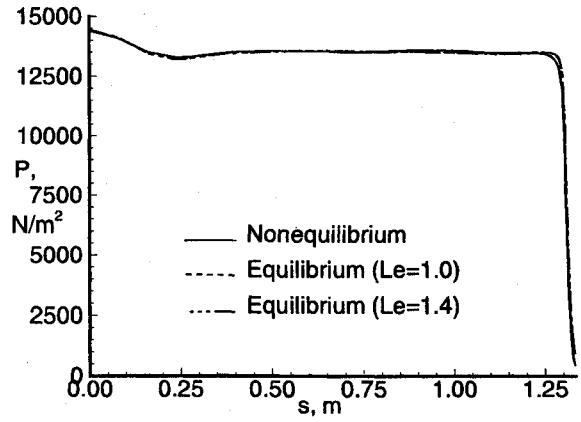

Fig. 2 Comparison of pressure distribution on the surface (V = 5.82 km/s, alt. = 37.9 km).

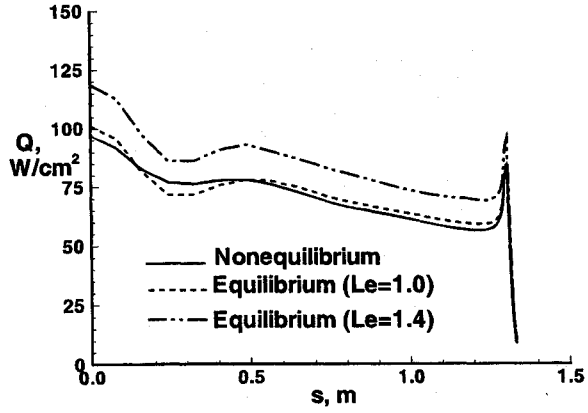

Fig. 3 Comparison of convective heating distribution on the surface (V = 5.82 km/s, alt. = 37.9 km).

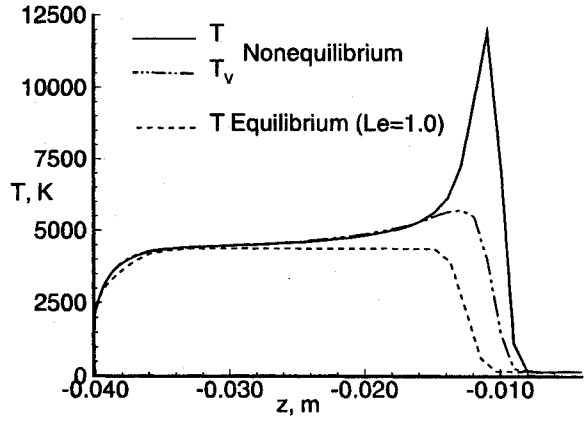

Fig. 4 Comparison of stagnation line temperature profiles (V = 5.82 km/s, alt. = 37.9 km).

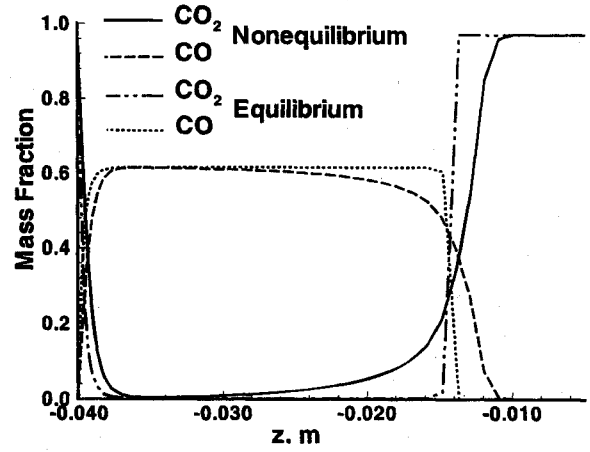

Fig. 5 Comparison of stagnation line mass fractions of CO_2 and CO (V = 5.82 km/s, alt. = 37.9 km).

of finite catalysis though the amount is unknown. Because of this uncertainty, the fully catalytic wall boundary condition is used. It will result in heating predictions which are the upper limit of those possible.

Additional comment concerning the use of a constant Lewis number in the equilibrium code is necessary. On the vehicle surface where the temperature is 2000 K and the pressure is 14,300 N/m^2, the equilibrium mass fraction of CO_2 is 0.94 which is close to its freestream value of 0.97. Thus, the gas at the wall predicted by an equilibrium calculation is comprised of recombined CO_2 and N_2. Using collision integrals from Lennard-Jones potentials for this binary pair, the Lewis number at the stagnation point conditions is computed to be 1.03. At a point in the middle of the shock layer where temperatures are 4400 K, the dominant species are CO and O. From this binary pair at the conditions in the middle of the shock layer, a Lewis number of 0.9 is computed. Thus, setting the Lewis number to a constant value of 1.0 for the entire layer is preferable to a value of 1.4. (The Le = 1.4 solution is included since this assumption has been used in recent Mars entry studies.[6,8])

The degree of nonequilibrium present in the shock layer is illustrated in Figs. 4 and 5. Figure 4 compares the temperature profiles from the two calculations along the stagnation line. Thermal nonequilibrium is restricted to a very small region behind the shock since that is the only place where the vibrational-electronic temperature does not equal the translational temperature. The degree of chemical nonequilibrium is indicated by the difference in T profiles. Additional indication of the degree of chemical equilibrium is shown in Fig. 5. This figure presents the stagnation line profiles of CO_2 and CO. (The freestream is on the right in the figure.) While it takes half of the shock layer for CO_2 to dissociate, the mass fractions of CO_2 and CO do reach their equilibrium values in the shock layer. Closer to the wall (at $z = -0.04$), the nonequilibrium solution's fully catalytic wall boundary condition forces rapid recombination so that the wall mass fractions equal those from the equilibrium method. A finite catalytic wall in the nonequilibrium calculation would produce less recombination than that shown in Fig. 5.

Table 3 Comparison of VSL solution with equilibrium and nonequilibrium solutions on stagnation streamline

	VSL	Eq. (Le = 1.4)	Eq. (Le = 1)	Noneq.
QW/cm^2	109.7	118.7	101.1	97.0
PN/m^2	14273	14441	14431	14392
T_{shock}K	4320	4380	4380	4800
δ_{shock}m	0.024	0.028	0.028	0.032

An equilibrium viscous-shock layer (VSL) solution (Le = 1.4) generated for the stagnation line of this case using the method of Ref. 8 is compared to the present Navier-Stakes calculations in Table 3. The solutions compare well. Stagnation-point convective heating predicted by the VSL is within 8 percent of the equilibrium (Le = 1.4) calculation and 12 percent of the nonequilibrium solution. The radiation calculation associated with this VSL method predicts the radiative heating to be 0.02 W/cm^2. (A second radiative heating prediction using the

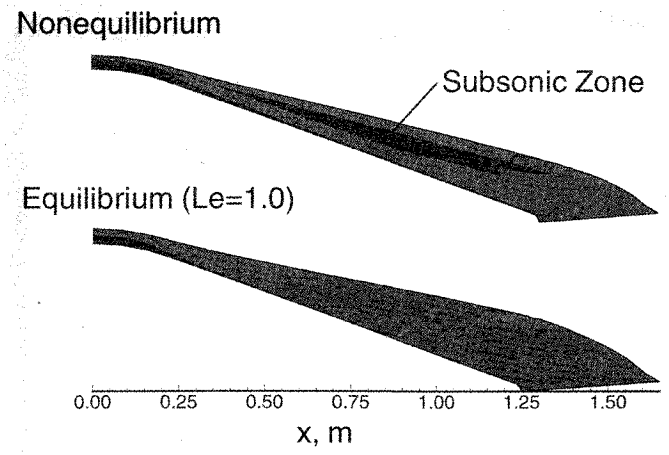

Fig. 6 Comparison of subsonic zone predicted by two calculations. (V = 5.82 km/s, alt. = 37.9 km).

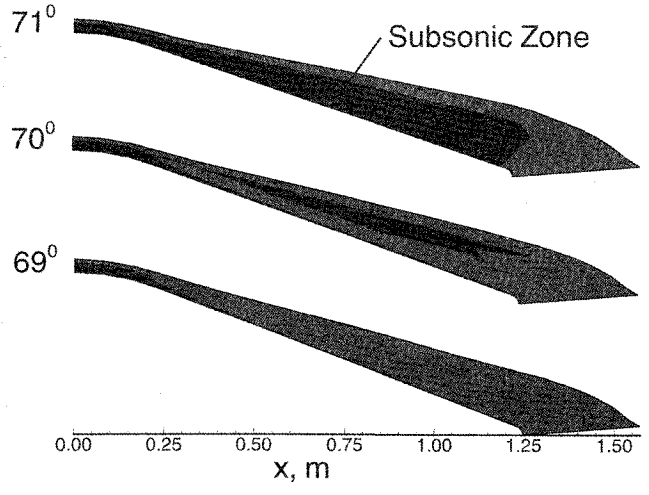

Fig. 7 Comparison of subsonic zone for different cone half-angles. (V = 5.82 km/s, alt. = 37.9 km).

method of Ref. 23 predicts a similarly negligible value of 0.03 W/cm^2.) Thus, radiative heating is negligible.

Information regarding the flow's character in the shock layer can be gained by examining the location of the sonic line. Figure 6 compares the subsonic zones predicted by the solutions. While the zone predicted by the equilibrium calculation is limited to the nose region, the nonequilibrium calculation shows signs of the zone shifting to the shoulder. (Mach number for the nonequilibrium plot uses the frozen speed of sound.) To examine this situation further, two additional nonequilibrium solutions are generated for these maximum heating point conditions. These two additional nonequilibrium solutions vary the cone half-angle of the vehicle's geometry: changing it from 70 deg to 69 and 71 deg, respectively. The subsonic zones for all three cone angles are compared in Fig. 7. Notice the sonic line has jumped to the shoulder for the 71-deg sphere cone. Thus, the entire forebody shock layer for that case is subsonic flow.

Two additional points on the 0.625-m-nose-radius, 70-deg sphere cone's trajectory are examined using the nonequilibrium code. The trajectory point two seconds before maximum heating occurs with velocity 6153 m/s at 41.5 km altitude (ρ_∞ = 0.29775e—03 kg/m^3, T_∞ = 161 K). The point two seconds after maximum heating occurs with a velocity of 5395 m/s at altitude 34.6 km (ρ_∞ = 0.618e−03 kg/m^3, T_∞ = 169 K). Figure

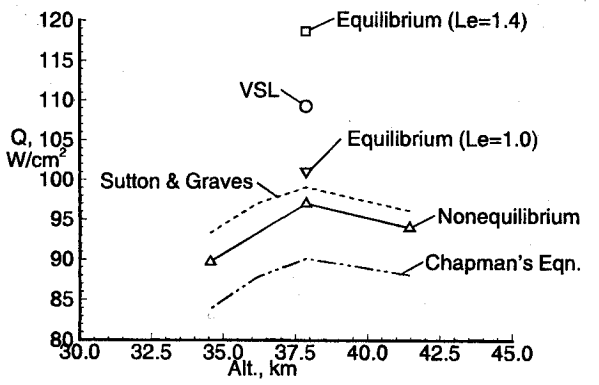

Fig. 8 Comparison of stagnation point heating from various methods at points near maximum heating on the 0.625-m body trajectory.

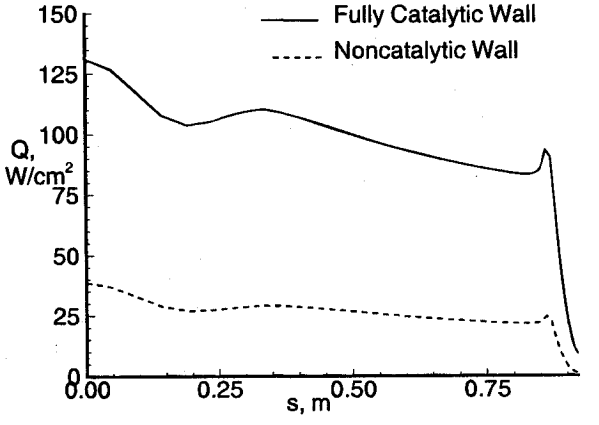

Fig. 9 Comparison of convective heating for different wall catalysis at conditions of Ref. 3.

8 presents stagnation-point heating vs altitude for these three nonequilibrium solutions (the three triangles) as well as the previously discussed equilibrium and VSL solutions. Results from two approximate heating predictions are also included in the figure. One is a modified Chapman's equation[13] described in the Introduction section and the second is a cold-wall correlation developed by Sutton and Graves.[24] This latter correlation for 97 percent CO_2 and 3 percent N_2 is

$$Q = 1.89e - 08\dot{R}_N^{-0.5}\rho_\infty^{0.5}V_\infty^3 \qquad (23)$$

where Q is in W/cm^2. Figure 8 reveals that predictions from the correlation of Sutton and Graves are within 4 percent of the present fully catalytic wall nonequilibrium calculation and the present equilibrium (Le = 1.0) calculation at peak heating.

Finally, the maximum heating point on the second (0.425-m-nose-radius body) trajectory of Ref. 3 is examined (V_∞ = 6155 m/s, ρ_∞ = 0.2687e—03 kg/m^3, T_∞ = 161 K). Figure 9 presents the convective heating predictions from the present nonequilibrium tool for this case. Both noncatalytic and fully catalytic wall boundary condition cases are shown. The effect of surface catalysis on heating is dramatic. At the stagnation point, the fully catalytic case predicts 131 W/cm^2; the noncatalytic result predicts 38 W/cm^2. The latter compares well with the prediction of 35 W/cm^2 in Ref. 3. The Sutton and Graves correlation[24] predicts 111 W/cm^2 for this case.

The method of Ref. 23 predicts that the radiative heating for this second trajectory's maximum heating point is, like that of the first trajectory, negligibly small.

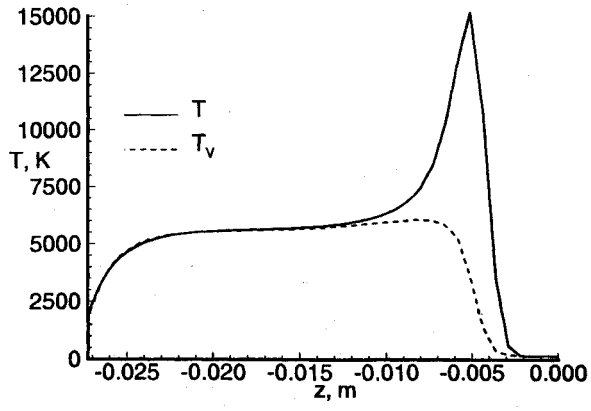

Fig. 10 Temperature profiles across the stagnation streamline for noncatalytic wall boundary condition. (V = 6.15 km/s, alt. = 41.7 km).

Figure 10 presents the stagnation line temperature profiles from the noncatalytic-wall solution. This case displays a small thermal nonequilibrium region behind the shock. Like the profiles shown in Fig. 4, the temperatures equilibrate so that T_V equals T for most of the shock layer. The rate of vibrational relaxation is the primary model which affects this equilibration process. However, another model has a strong effect on this equilibration: the amount of vibrational energy removed when a molecule dissociates.

For Earth entries, this energy exchange model is often set to the average vibrational energy of the local flow. If the average amount is used for the Mars entries examined, T_V does not behave as shown in Fig. 10. Rather, T_V grows larger than T behind the shock: an implausible result for this compressive flow. Such an overshoot is prevented—and the results of Figs. 4 and 10 generated—if the amount of vibrational energy removed due to dissociation is set to ten times the average local vibrational energy. This is an assumption of preferential dissociation, but the selection of the factor ten has little justification. Furthermore, other values for this parameter (e.g., the dissociation energy for the molecule or that less the molecule's translational energy) might also have proved acceptable.

The effect of surface catalysis on heating is dramatic. When the 0.625-m-nose-radius vehicle case was recomputed assuming a noncatalytic wall boundary condition at 1500 K, the stagnation point heating rate dropped from 97 to 34 W/cm^2. This behavior was observed in Ref. 2.

The computational cost of the equilibrium code is three times that of the nonequilibrium code. In Cray-YMP CPU time, a nonequilibrium calculation requires 20 minutes while the equilibrium requires one hour. This unexpected ratio is a result of the Newton iteration required by the equilibrium thermodynamics. The problem is exacerbated by the inclusion of 19 species in the equilibrium method. If only eight were considered (as in the nonequilibrium method) the equilibrium calculation's cost is cut in half. Most equilibrium calculations for Earth entries are an order of magnitude faster because they utilize curve fits to specify the mixture thermodynamics and transport properties.[16]

Conclusions

The computational-fluid-dynamic models for the thermodynamics and transport properties presented in this paper and incorporated into the Langley aerothermodynamics upwind relaxation algorithm (LAURA) are viable means of predicting Mars atmospheric-entry flowfields. Application of both methods, the equilibrium thermochemistry code and the two-temperature nonequilibrium thermochemistry code, to conditions characteristic of the Mars environmental survey mission (MESUR) result in the following conclusions concerning the aerothermodynamics of MESUR Mars entry.

The flowfield around a 0.625-m-nose-radius sphere cone traveling 5819 m/s at 37.9 km altitude is characterized by near-equilibrium conditions, though chemical nonequilibrium effects are present behind the shock.

The sonic line for this 70 deg half-angle body sits at the sphere-cone tangency point. If, however, the cone half-angle is increased to 71 deg, the sonic line moves aft to the shoulder. This shift might also occur on the windward side of the 70 deg body at angle of attack.

Use of a Lewis number of 1.0 to define the diffusion coefficient in the equilibrium thermochemistry code is supportable and results in surface heating predictions near that predicted by the nonequilibrium code which defines its diffusion coefficients from collision integrals.

Convective heating at the stagnation point is predicted to be 101 W/cm^2 by the equilibrium code and 97 W/cm^2 by the nonequilibrium code using a fully catalytic wall boundary condition. The approximate heating correlation of Sutton and Graves predicts a value of 99.1 W/cm^2. These predictions should represent the upper limit of possible heating. Radiative heating is negligible.

Use of a noncatalytic wall boundary condition decreases the predicted convective heating. For a 0.425-m-nose-radius, 70 deg sphere cone traveling 6155 m/s at 41.7 km altitude, this switch in nonequilibrium wall boundary condition causes the heating prediction to drop from 131 to 38 W/cm^2. The noncatalytic result represents the lower limit on the expected heating. More precise predictions will require knowledge of the surface catalysis of the proposed thermal protection system.

The amount of vibrational energy removed when a molecule dissociates—or added when it recombines—has an impact on the equilibration of temperatures in the nonequilibrium solutions. The value of a constant in this model selected as appropriate for the Mars atmosphere is ten times larger than that used in air calculations.

Acknowledgments

Sincere thanks are extended to Peter Gnoffo, Roop Gupta, and Kam-Pui Lee for their help in performing this research. Dick Powell and Robert Braun supplied the trajectory and maximum heating point for the 0.625-m MESUR mission.

References

[1] Hubbard, G. S., Wercinski, P. F., Sarver, G. L., Hanel, R. P., and Ramos, R., "A Mars Environmental Survey (MESUR)—Feasibility of a Low Cost Global Approach," International Aeronautical Federation Paper 91-432, Oct. 1991.

[2] Chen, Y. -K., Henline, W. D., Stewart, D. A., and Candler, G. V., "Navier-Stokes Solutions with Surface Catalysis for Martian Atmospheric Entry," AIAA Paper 92-2946, July 1992.

[3] Tauber, M., Henline, W., Chargin, M., Papadopoulos, P., Chen, Y., Yang, L., and Hamm, K., "MESUR Probe Aerobrake Preliminary Design Study," AIAA Paper 92-2952, July 1992.

[4] Papadopoulos, P., Tauber, M., and Chang, I. -D., "Aerobraking in a Dusty Martian Atmosphere," AIAA Paper 90-1700, June 1990.

[5] Park, C., Howe, J. T., Jaffe, R. L., and Candler, G. V., "Chemical Kinetic Problems of Super-Escape Velocity Mars Entries: A Review and Extension," AIAA Paper 91-0464, Jan. 1991.

[6] Candler, G. V., "Computation of Thermochemical Nonequilibrium Martian Atmospheric Entry Flows," AIAA Paper 90-1695, June 1990.

[7] Rock, S. G., and Candler, G. V., "Analysis of Thermo-Chemical Nonequilibrium Models for Carbon Dioxide Flows," AIAA Paper 92-2852, July 1992.

[8] Gupta, R. N., Lee, K. P., Moss, J. N., and Sutton, K., "A Viscous-Shock-Layer Analysis of the Martian Aerothermal Environment," AIAA Paper 91-1345, June 1991.

[9] Legner, H. H., Baker, J. E., Mulhall, P. A., and Cronin, J. F., "Martian Atmosphere Boundary Layer Code," AIAA Paper 91-1346, June 1991.

[10] Gnoffo, P. A., Gupta, R. N., and Shinn, J. L., "Conservation Equations and Physical Models for Hypersonic Air Flows in Thermal and Chemical Nonequilibrium," NASA TP-2867, Feb. 1989.

[11] Gnoffo, P. A., "An Upwind-Biased, Point-Implicit Relaxation Algorithm for Viscous, Compressible Perfect-Gas Flows," NASA TP-2953, Feb. 1990.

[12] Bauer, G. L., Cornick, D. E., and Stevenson, R., "Capabilities and Applications of the Program to Optimize Simulated Trajectories (POST)", NASA CR-2770, 1977.

[13] Chapman, D. R., "An Approximate Analytical Method for Studying Entry into Planetary Atmospheres," NASA TR R-11, 1959.

[14] Gupta, R. N., Yos, J. M., Thompson, R. A., and Lee, K. P., "A Review of Reaction Rates and Thermodynamic and Transport Properties for an 11-Species Air Model for Chemical and Thermal Nonequilibrium Calculations to 30000 K," NASA RP-1232, Aug. 1990.

[15] Stroud, C. W., and Brinkley, K. L., "Chemical Equilibrium of Ablation Materials Including Condensed Species," NASA TN D-5391, Aug. 1969.

[16] Greene, F. A., "Viscous Equilibrium Computations Using Program LAURA," AIAA Paper 91-1389, June 1991.

[17] Wilke, C. R., "A Viscosity Equation for Gas Mixtures," *Journal of Chemical Physics*, Vol. 18, No. 4, 1950, p. 517.

[18] Mason, E. A., and Saxena, S. C., "Approximate Formula for the Thermal Conductivity of Gas Mixtures," *The Physics of Fluids*, Vol. 1, No. 5, 1958, pp. 361–369.

[19] Hirschfelder, J. O., Curtiss, C. F., and Bird, R. B., *Molecular Theory of Gases and Liquids*, John Wiley and Sons, Inc., New York, 1954, pp 558.

[20] Millikan, R. C., and White, D. R., "Systematics of Vibrational Relaxation," *Journal of Chemical Physics*, Vol. 39, No. 12, 1963, pp. 3209–3213.

[21] Camac, M., "CO_2 Relaxation Processes in Shock Waves," *Fundamental Phenomena in Hypersonic Flow*, edited by J. G. Hall, Cornell Univ. Press, Ithaca, NY, 1966, pp. 195–215.

[22] Hartung, L. C., Mitcheltree, R. A., and Gnoffo, P. A., "Stagnation Point Radiative Heating and the Influence of Energy Exchange Models," *Journal of Thermophysics and Heat Transfer*, Vol. 6, No. 3, 1992, pp. 412–418.

[23] Hartung, L. C., Sutton, K., and Brauns, F., "Equilibrium Radiative Heating Tables for Aerobraking in the Martian Atmosphere," NASA TM-102659, May, 1990.

[24] Sutton, K., and Graves, R. A., "A General Stagnation-Point Convective-Heating Equation for Arbitrary Gas Mixtures," NASA TR R-376, Nov. 1971.

K. James Weilmuenster
Associate Editor